Superconductivity from repulsive interactions in rhombohedral trilayer graphene: A Kohn-Luttinger-like mechanism

Tommaso Cea ⬤ and Pierre A. Pantaleón ⬤
Imdea Nanoscience, Faraday 9, 28015 Madrid, Spain

Võ Tiến Phong
Department of Physics and Astronomy, University of Pennsylvania, Philadelphia PA 19104, USA

Francisco Guinea
Imdea Nanoscience, Faraday 9, 28015 Madrid, Spain;
Donostia International Physics Center, Paseo Manuel de Lardizábal 4, 20018 San Sebastián, Spain;
and Ikerbasque, Basque Foundation for Science, 48009 Bilbao, Spain

We study the emergence of superconductivity in rhombohedral trilayer graphene due purely to the long-range Coulomb repulsion. This repulsive-interaction-driven phase in rhombohedral trilayer graphene (RTG) is significantly different from those found in twisted bilayer and trilayer graphenes. In the latter case, the nontrivial momentum-space geometry of the Bloch wave functions contributes to an effective attractive electron–electron interaction; this allows for less modulated order parameters and for spin-singlet pairing. In RTG, we instead find spin-triplet superconductivity with critical temperatures up to ∼0.15 K. The critical temperatures strongly depend on electron filling and peak where the density of states diverge. The order parameter shows a significant modulation within each valley pocket of the Fermi surface.

I. INTRODUCTION

Recently, superconductivity was experimentally observed in a three-layer graphene stack with rhombohedral (ABC) arrangement that is tunable by an applied interlayer bias [1]. Following this, several theories have been proposed to account for the onset of effective attractive interaction between electrons mediated by different pairing mechanisms: Electron-phonon coupling [2], spin fluctuations near an antiferromagnetic phase [3,4], direct coupling by the screened Coulomb interaction [5], or pairing mediated by the proximity to a correlated metal [4,6]. Although different in details, all of these proposals made use of the fact that the density of states (DOS) of ABC trilayer graphene near charge neutrality can be greatly enhanced by applying a gate voltage across the three layers. Ignoring possible weak spin-orbit couplings, intrinsic ABC trilayer graphene is a semimetal with an approximate cubic band degeneracy at the zone corners [7–24]. When resolved close to these points, the cubic degeneracy actually splits into three Dirac cones, creating a trigonally warped Fermi surface (FS). As a perpendicular electric field is applied, inversion symmetry is broken, and these Dirac points acquire a finite mass. As a result, the local band dispersion can be nearly quenched, generating a van Hove singularity that favors the emergence of correlated electronic phases.

Similar physics can also be found in three-dimensional (3D) rhombohedral graphite, which is a nodal line semimetal that has a flat electronic band at the top and bottom surfaces of a sufficiently wide stack [25]. The associated divergent DOS is expected to enhance electron–electron interactions and lead to broken-symmetry phases, including superconductivity [13,14] and magnetism [16]. Experimentally, gaps and broken-symmetry phases in finite rhombohedral stacks have been reported [15,17–19,21–24]. The partially flat bands in rhombohedral stacks make these systems spectrally similar to magic-angle twisted bilayer graphene [26,27], importantly without the need for a superlattice structure.

Inspired by these observations, we analyze here the appearance of superconductivity in rhombohedral trilayer graphene (RTG). We assume that the only electron–electron coupling is via the long-range Coulomb interaction. We analyze the possibility of pairing using a diagrammatic technique, similar to the Kohn-Luttinger approach [28] to superconductivity due to repulsive interactions (see also Ref. [5]). The same scheme has been already applied to twisted bilayer graphene [29] and to twisted trilayer graphene [30]. The use of the same technique allows us to compare the emergence of superconductivity in twisted and rhombohedral stacks. As discussed below, the calculation leads to superconducting (SC) phases in both types of materials, although the physical origin of superconductivity and the SC order parameter (OP) are significantly different in the two cases.

A. Tight-binding Hamiltonian

The 3D crystal structure of RTG is shown in Fig. 1(a). Each unit cell consists of six carbon atoms, two per layer, connected to each other via hopping amplitudes as shown in Fig. 1(b).

The minimal tight-binding Hamiltonian is given by [10]

$$H_{tb}(\vec{k}) = \begin{pmatrix} \Delta_1 + \Delta_2 & -\gamma_0 u(\vec{k}) & \gamma_4 u^*(\vec{k}) & \gamma_1 & 0 & 0 \\ -\gamma_0 u^*(\vec{k}) & \Delta_1 + \Delta_2 + \delta & \gamma_3 v(\vec{k}) & \gamma_4 u^*(\vec{k}) & \gamma_2/2 & 0 \\ \gamma_4 u(\vec{k}) & \gamma_3 v^*(\vec{k}) & -2\Delta_2 & -\gamma_0 u(\vec{k}) & \gamma_4 v^*(\vec{k}) & \gamma_1 \\ \gamma_1 & \gamma_4 u(\vec{k}) & -\gamma_0 u^*(\vec{k}) & -2\Delta_2 & \gamma_3 u(\vec{k}) & \gamma_4 u^*(\vec{k}) \\ 0 & \gamma_2/2 & \gamma_4 v(\vec{k}) & \gamma_3 u^*(\vec{k}) & \Delta_2 - \Delta_1 + \delta & -\gamma_0 v(\vec{k}) \\ 0 & 0 & \gamma_1 & \gamma_4 u(\vec{k}) & -\gamma_0 v^*(\vec{k}) & \Delta_2 - \Delta_1 \end{pmatrix}, \qquad (1)$$

where γ_i are the hopping amplitudes, Δ_1 is a potential difference between nearest-neighbor layers which takes into account an external displacement field, Δ_2 is the potential difference between the middle layer compared with mean potential of the outer layers, δ encodes an on-site potential which is only present at sites B_1 and A_3 since these two atoms do not have a neighbor on the middle layer, and $u(\vec{k}) = 1 + 2\cos(k_x a/2)e^{-ik_y a\sqrt{3}/2}$, $v(\vec{k}) = e^{ik_y a\sqrt{3}}u(\vec{k})$, with $a = 2.46$ Å is the lattice constant of graphene. The optimal values of the minimal tight-binding parameters, γ_i and δ, have been reported in the literature [10,11,19,20,23,31]. Here we use the ones calculated in Refs. [24,31]. These parameters are tabulated in Table I.

Details concerning the single-particle band structure corresponding to model (1) are provided in the Supplemental Material [32].

B. Long-range Coulomb interaction and internal screening

To account for electron–electron interactions, we assume that two electrons separated by a distance r experience a r^{-2} long-range Coulomb repulsion

$$V_C(r) = \frac{e^2}{4\pi\epsilon_0\epsilon r}, \quad \text{for } r \neq 0,$$
$$V_C(0) = \frac{w_0}{\epsilon}, \qquad (2)$$

where e is the electron charge, ϵ_0 is the dielectric constant of vacuum, and ϵ is the relative dielectric constant of the environment. In this work, we set $\epsilon = 4$, which reproduces accurately the screening by a substrate of hexagonal boron nitride (hBN). The parameter w_0 accounts for the local repulsion, which we set to $w_0 = 17$ eV following Ref. [33]. As the potential V_C varies slowly on the atomic scale, we approximate the interaction between two electrons as only depending on the distance between the centers of the two unit cells in which the electrons reside. In reciprocal space, V_C is given by

$$V_C(\vec{q}) = \sum_{\vec{R}} V_C(|\vec{R}|)e^{-i\vec{q}\cdot\vec{R}}, \qquad (3)$$

where $\vec{q} \in$ BZ, the sum runs over all positions $\vec{R}$ of the lattice, with a periodic boundary condition imposed by the finite grid used to sample the BZ.

In order to describe internal screening due to particle-hole excitations, we use the static random-phase approximation (RPA), leading to the usual renormalization of V_C

$$V_{scr}(\vec{q}) = \frac{V_C(\vec{q})}{1 - V_C(\vec{q})\Pi(\vec{q})}, \qquad (4)$$
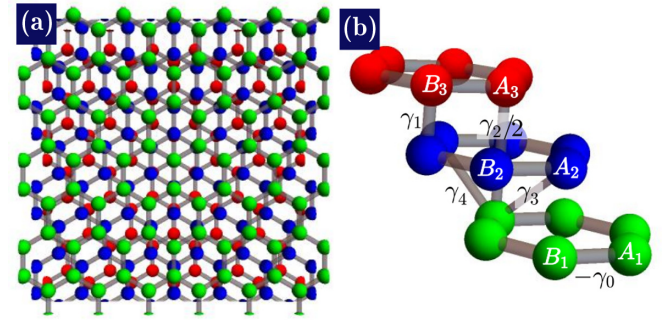

FIG. 1. Lattice structure of ABC RTG. (a) The 3D crystal structure viewed from the top. (b) Some representative hopping parameters between carbon atoms.

where $\Pi(\vec{q})$ is the zero-frequency limit of the charge susceptivity, as given by

$$\Pi(\vec{q}) = \frac{2}{N_c} \sum_{\vec{k}nm} \frac{f(\xi_{n,\vec{k}}) - f(\xi_{m,\vec{k}+\vec{q}})}{\epsilon_{n,\vec{k}} - \epsilon_{m,\vec{k}+\vec{q}}}$$
$$\times |\langle\vec{\psi}_{m,\vec{k}+\vec{q}}|\vec{\psi}_{n,\vec{k}}\rangle|^2, \qquad (5)$$

where N_c is the number of unit cells, $\epsilon_{n,\vec{k}}$ is the n-th band energy at wave-vector $\vec{k}$, $\vec{\psi}_{n,\vec{k}}$ is the corresponding six-component eigenvector, $f(\xi) = [1 + e^{\xi/(K_B T)}]^{-1}$ is the Fermi-Dirac distribution at the temperature T, $\xi_{n,\vec{k}} = \epsilon_{n,\vec{k}} - \mu$, and μ is the chemical potential. The factor of two in front of Eq. (5) accounts for spin degeneracy. As an example, Fig. 2 shows the profiles of (a) the inverse of the dielectric function, $\kappa^{-1}(\vec{q}) = [1 - V_C(\vec{q})\Pi(\vec{q})]^{-1}$, and (b) the screened potential, $V_{scr}(\vec{q})$, computed along a high-symmetry path of the BZ (see the Supplemental Material) and obtained for $\Delta_1 = 50$ meV and electronic density $n_e = -1.91\times10^{12}$ cm^{-2}. To perform the calculation, we used $N_c = 12\times10^4$, which is enough to finely resolve the band structure close to the FS. The results display an overall strong screening. Remarkably, $V_{scr}(\vec{q})$ vanishes at the center of the BZ, the point Γ, which means that $\Pi(\vec{q})$ diverges as $\vec{q} \to 0$ and implies that V_{scr} is locally attractive in real space. This is shown in the inset of Fig. 2(b), displaying the real-space profile of the screened potential

TABLE I. Minimal tight-binding parameters of RTG expressed in eV (see also Refs. [24,31]).

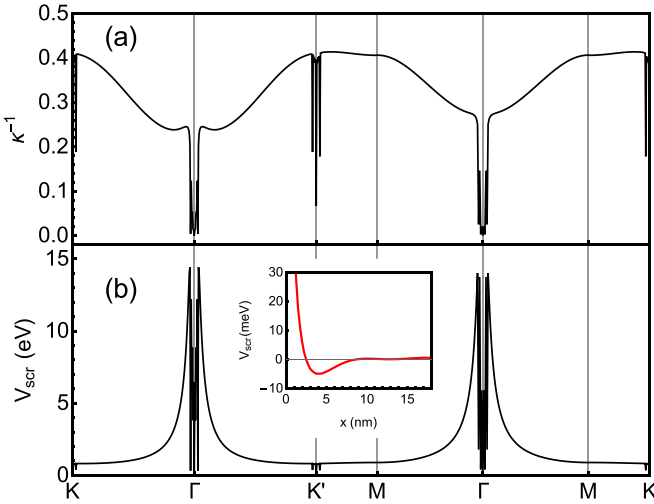| γ_0	γ_1	γ_2	γ_3	γ_4	δ	Δ_2
3.1	0.38	−0.015	0.29	0.141	−0.0105	−0.0023

FIG. 2. Screened Coulomb potential. (a) Inverse of the dielectric function, $\kappa^{-1}(\vec{q}) = [1 - V_C(\vec{q})\Pi(\vec{q})]^{-1}$. (b) Screened potential, $V_{scr}(\vec{q})$. The inset shows the real-space profile of the screened potential computed along the horizontal axis, x. The profiles are computed along a high-symmetry path of the BZ and obtained for $\Delta_1 = 50$ meV and electronic density $n_e = -1.91 \times 10^{12}$ cm^{-2}.

computed along the horizontal axis, x, and which clearly identifies an attractive minimum at the interparticle distance of $x \sim 3$ nm.

C. Superconductivity

Next we assume that the interaction which leads to pairing in RTG is the long-range Coulomb interaction (Ref. [5] makes the same assumption). The calculations carried out in Refs. [29,30] include, for completeness, the coupling of electronic charge oscillations to longitudinal phonons, as these phonons modify the screening of the Coulomb interaction. It is interesting to note that the inclusion of longitudinal phonons does not change significantly the results reported here.

The critical temperature for the onset of superconductivity in RTG can be obtained from the linearized gap equation

$$\Delta_{ij}(\vec{k}) = -\frac{K_B T}{N_c} \sum_{\vec{k}'\omega} \sum_{i'j'} V_{scr}(\vec{k} - \vec{k}')$$

$$\times G_{ii'}(\vec{k}', i\hbar\omega) G_{jj'}(-\vec{k}', -i\hbar\omega) \Delta_{i'j'}(\vec{k}'), \quad (6)$$

where ω are fermionic Matsubara frequencies; i, i', j, j' label the sublattice/layer degree of freedom; and $G_{ii'}(\vec{k}, i\hbar\omega)$ is the normal-state single-particle Green's function

$$G_{ii'}(\vec{k}, i\hbar\omega) = \sum_n \frac{\psi^i_{n,\vec{k}} \psi^{i',*}_{n,\vec{k}}}{i\hbar\omega - \xi_{n,\vec{k}}}. \quad (7)$$

Our framework is similar to the Kohn-Luttinger scheme [28]. The approach in Ref. [28] includes all processes up to second order in perturbation theory. Our approach neglects exchange-like diagrams but on the other hand includes all bubble diagrams to infinite orders. The multiplicity of these diagrams is equal to the number of electron flavors, in the present case

$\mathcal{N}_f = 2$. Hence it can be considered an expansion in powers of $\mathcal{N}_f^{-1}$.

On projecting Eq. (6) onto the band basis and performing the Matsubara sum, we rewrite it as

$$\Delta_{m_1 m_2}(\vec{k}) = \sum_{\vec{k}' n_1 n_2} \Gamma_{m_1 m_2, n_1 n_2}(\vec{k}, \vec{k}') \Delta_{n_1 n_2}(\vec{k}'), \quad (8)$$

where

$$\Delta_{m_1 m_2}(\vec{k}) = \sum_{ij} \psi^{i,*}_{m_1,\vec{k}} \psi^i_{m_2,\vec{k}} \Delta_{ij}(\vec{k})$$

$$\times \sqrt{\frac{f(-\xi_{m_2,\vec{k}}) - f(\xi_{m_1,\vec{k}})}{\xi_{m_2,\vec{k}} + \xi_{m_1,\vec{k}}}}, \quad (9)$$

and $\Gamma_{m_1 m_2, n_1 n_2}(\vec{k}, \vec{k}')$ is the Hermitian kernel

$$\Gamma_{m_1 m_2, n_1 n_2}(\vec{k}, \vec{k}')$$

$$= -\frac{1}{N_c} V_{scr}(\vec{k} - \vec{k}') \langle \vec{\psi}_{m_1,\vec{k}} | \vec{\psi}_{n_1,\vec{k}'} \rangle \langle \vec{\psi}_{n_2,\vec{k}'} | \vec{\psi}_{m_2,\vec{k}} \rangle$$

$$\times \sqrt{\frac{f(-\xi_{m_2,\vec{k}}) - f(\xi_{m_1,\vec{k}})}{\xi_{m_2,\vec{k}} + \xi_{m_1,\vec{k}}}} \sqrt{\frac{f(-\xi_{n_2,\vec{k}'}) - f(\xi_{n_1,\vec{k}'})}{\xi_{n_2,\vec{k}'} + \xi_{n_1,\vec{k}'}}}. \quad (10)$$

We make use of the time-reversal symmetry of Hamiltonian (1), which implies $\xi_{n,-\vec{k}} = \xi_{n,\vec{k}}$ and $\vec{\psi}_{m,-\vec{k}} = \vec{\psi}^*_{m,\vec{k}}$. At a critical temperature, T_c, the largest eigenvalue of the kernel $\Gamma_{m_1 m_2, n_1 n_2}(\vec{k}, \vec{k}')$ is 1. The corresponding eigenvector provides the symmetry of the OP.

We diagonalize numerically the kernel of Eq. (10). As the leading contribution to Eq. (8) comes from the states closest to the FS, we cut off phase space by considering only the states satisfying $|\xi_{n,\vec{k}}| \leqslant w$, with $w = 30$ meV. In order to rule out finite-size effects and to finely sample the FS at densities on the order of $\sim 10^{12}$ cm^{-2}, we implement a length renormalization: $a \rightarrow a_s = s \times a$, where $s > 1$ is the scale factor and a_s is the effective lattice spacing. This procedure defines an effective tight-binding model where the hopping amplitudes γ_0, γ_3, and γ_4 are rescaled according to $\gamma_i \rightarrow \gamma_{i,s} = \gamma_i/s$, $i = 0, 3, 4$. This procedure reduces the size of the BZ by a factor of s^2, allowing us to study considerably larger meshes that would otherwise be numerically prohibitive. In doing so, we are able to obtain a finer momentum resolution close to the charge neutrality point (CNP) to improve accuracy.

D. Critical SC temperature

Figure 3 shows the value of the critical temperature as a function of electronic density, n_e, for $\Delta_1 = 0$, 50, 75, 100, and 125 meV. The results are obtained with a grid of 3×10^4 points in the BZ on rescaling with $s = 10$, meaning that we are considering 3×10^6 unit cells of the atomic RTG. The critical temperatures feature pronounced maxima on the order of $0.1 - 0.2$ K for finite values of Δ_1. In contrast, we do not observe any appreciable enhancement of T_c without a bias. To gain insight into this behavior, we show in Fig. 4 the bands (a) and DOS (b) close to the CNP obtained for some of the values of Δ_1 considered in Fig. 3. We observe that a finite bias significantly enhances the van Hove singularities near the
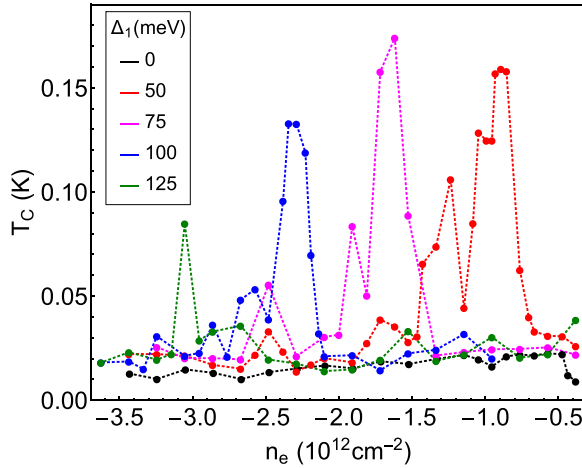
FIG. 3. Critical temperature as a function of filling for various values of the interlayer bias.

FIG. 5. Symmetry of the SC OP in the vicinity of K and K'. These are calculated for $\Delta_1 = 50$ meV and $n_e = -1.14 \times 10^{12}$ cm^{-2} (a) and -1.91×10^{12} cm^{-2} (b). The black lines identify the FS.

band edge, a feature that is absent in the zero-bias limit. In Fig. 4, the horizontal dashed lines identify the Fermi levels corresponding to the values of n_e which maximize T_c in Fig. 3. These Fermi energies match the position of the Van Hove singularities with great accuracy, showing that superconductivity is strongly enhanced when the Fermi level is close to a peak in the DOS. In addition, given a finite bias, a sizable T_c survives only in a narrow region of n_e around an optimal value, thus providing a tool to trigger superconductivity by tuning n_e and/or Δ_1. It is worth noting that the results reported in Fig. 3 are in reasonable agreement with the experimental data of Ref. [1] in terms of both the magnitude of the critical temperatures and the range of densities reported.

E. Symmetry of the SC OP

Finally, we study the SC OP. Figure 5 shows the symmetry of the SC OP in the vicinity of K and K', obtained for $\Delta_1 = 50$ meV and $n_e = -1.14, -1.91 \times 10^{12}$ cm^{-2}, which are representative of most of the cases we have studied. The black lines identify the FS. These results have been obtained without
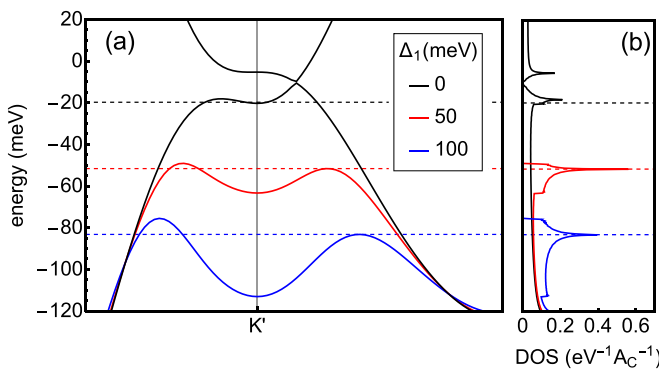
scaling, $s = 1$, by using $N_c = 12 \times 10^4$ unit cells of the atomic RTG. As expected, the OP is nonzero only in a narrow region of the BZ around the FS, implying that only the electrons close to the Fermi level participate in Cooper pairing. In addition, the OP clearly displays A_2 symmetry, meaning that it is antisymmetric on exchanging $\vec{k} \to -\vec{k}$. Because Hamiltonian (1) is spin degenerate and the interaction, Eq. (2), does not couple different spin flavors, the gap Eqs. (6) and (8) do not contain explicitly the spin indices, implying that they cannot distinguish between spin-triplet and spin-singlet superconductivity. However, A_2 symmetry necessarily implies that the Cooper pairs must be spin triplets in order for their wave function to be antisymmetric on exchanging the two electrons [34]. In the experiment in Ref. [1], two distinct SC transitions have been found, called SC1 and SC2, where the latter occurs in a magnetic phase and violates the Pauli's limit. As we are not accounting for the magnetic ordering, our analysis seems to be appropriate to describe the more conventional SC1 transition, whose observed critical temperatures are of the same order of magnitude as those in Fig. 3. It is worth noting that the spin triplet that we find is not in contradiction to the Pauli's limit, to which SC1 obeys, provided that the two electrons have opposite spin orientation. For instance, the A and B phases of superfluid ^{3}He belong to this category. There is no obvious reason to assume that the SC1 phase is not of this type (on the other hand, the A1 phase of ^{3}He describes spin-polarized Cooper pairs, as in phase SC2). Finally, we note that the OP changes sign within each valley pocket of the FS. The pairing potential represented by the kernel $\Gamma_{m_1 m_2, n_1 n_2}(\vec{k}, \vec{k}')$, Eq. (10), is repulsive in reciprocal space, and the eigenvector corresponding to the eigenvalue 1 cannot have a constant sign. This is a general feature of weak-coupling superconductivity induced by electronic interactions, where the SC wave function displays a high angular momentum, as is the case for p- or f-wave superconductivity.

II. CONCLUSIONS

We have analyzed diagrammatically the existence of superconductivity in RTG. We assume that the leading electron–electron interaction is Coulomb repulsion. Our results show that this interaction is enough to induce superconductivity in RTG, although it cannot be excluded that other excitations can contribute [2–4,6]. The large DOS in RTG at low

FIG. 4. Bias-induced van Hove singularities. Electronic bands (a) and DOS (b) close to the CNP, obtained for the values of Δ_1 considered in Fig. 3. The horizontal dashed lines identify the Fermi levels corresponding to the values of n_e which maximize T_c in Fig. 3.
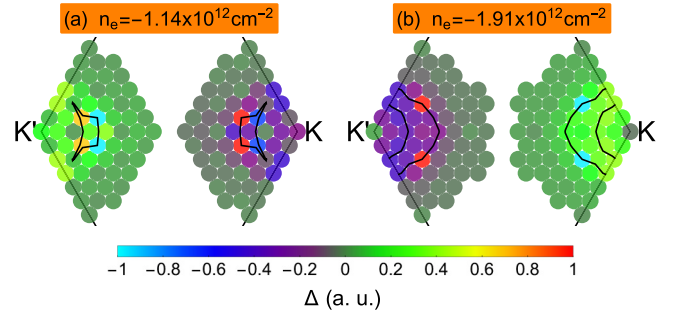
fillings leads to a significant screening of the interaction. The screened Coulomb repulsion induces superconductivity with critical temperatures upward ~ 0.15 K that depend strongly on electron filling and are correlated with peaks in the DOS. The OP fluctuates in sign within each valley, in agreement with the existence of a repulsive interaction at small momenta. Overall, the OP is antisymmetric in the BZ, so that the pairs must be spin triplets. The method used here has also been applied to the study of superconductivity in twisted bilayer and trilayer graphene [29,30]. In those cases, however, the OP does not change its sign and the superconductivity can be spin singlet/valley triplet or spin triplet/valley singlet. The small momentum modulation of the OP implies that long-range disorder is pair breaking in RTG, while that is not the case in twisted bilayer/trilayer graphene. Our analysis does not consider the magnetic ordering and hence it is more appropriate to describe the SC1 transition observed in Ref. [1]. We leave the study of the SC2 transition to a future work.

[1] H. Zhou, T. Xie, T. Taniguchi, K. Watanabe, and A. F. Young, Superconductivity in rhombohedral trilayer graphene, Nature (London) **598**, 434 (2021).

[2] Y.-Z. Chou, F. Wu, J. D. Sau, and S. Das Sarma, Acoustic-Phonon-Mediated Superconductivity in Rhombohedral Trilayer Graphene, Phys. Rev. Lett. **127**, 187001 (2021).

[3] H. Dai, J. Hou, X. Zhang, Y. Liang, and T. Ma, Mott insulating state and d +i d superconductivity in an ABC graphene trilayer, Phys. Rev. B **104**, 035104 (2021).

[4] Z. Dong and L. Levitov, Superconductivity in the vicinity of an isospin-polarized state in a cubic Dirac band, arXiv:2109.01133.

[5] A. Ghazaryan, T. Holder, S. Maksym, and E. Berg, Unconventional Superconductivity in Systems with Annular Fermi Surfaces: Application to Rhombohedral Trilayer Graphene, Phys. Rev. Lett. **127**, 247001 (2021).

[6] S. Chatterjee, T. Wang, E. Berg, and M. P. Zaletel, Inter-valley coherent order and isospin fluctuation mediated superconductivity in rhombohedral trilayer graphene, arXiv:2109.00002.

[7] J. W. McClure, Electron energy band structure and electronic properties of rhombohedral graphite, Carbon **7**, 425 (1969).

[8] M. S. Dresselhaus and G. Dresselhaus, Intercalation compounds of graphite, Adv. Phys. **51**, 1 (2002).

[9] D. P. Arovas and F. Guinea, Stacking faults, bound states, and quantum hall plateaus in crystalline graphite, Phys. Rev. B **78**, 245416 (2008).

[10] F. Zhang, B. Sahu, H. Min, and A. H. MacDonald, Band structure of *abc*-stacked graphene trilayers, Phys. Rev. B **82**, 035409 (2010).

[11] M. Koshino, Interlayer screening effect in graphene multilayers with *aba* and *abc* stacking, Phys. Rev. B **81**, 125304 (2010).

[12] W. Bao, L. Jing, J. Velasco Jr., Y. Lee, D. Liu, G.and Tran, B. Standley, M. Aykol, S. B. Cronin, D. Smirnov, M. Koshino, E. McCann, M. Bockrath, and C. N. Lau, Stacking-dependent band gap and quantum transport in trilayer graphene, Nat. Phys. **7**, 948 (2011).

[13] N. B. Kopnin, T. T. Heikkilä, and G. E. Volovik, High-temperature surface superconductivity in topological flat-band systems, Phys. Rev. B **83**, 220503(R) (2011).

[14] N. B. Kopnin, M. Ijäs, A. Harju, and T. T. Heikkilä, High-temperature surface superconductivity in rhombohedral graphite, Phys. Rev. B **87**, 140503(R) (2013).

[15] Y. Lee, D. Tran, K. Myhro, J. Velasco, N. Gillgren, C. N. Lau, Y. Barlas, J. M. Poumirol, D. Smirnov, and F. Guinea, Competition between spontaneous symmetry breaking and single-particle gaps in trilayer graphene, Nat. Commun. **5**, 5656 (2014).

[16] B. Pamuk, J. Baima, F. Mauri, and M. Calandra, Magnetic gap opening in rhombohedral-stacked multilayer graphene from first principles, Phys. Rev. B **95**, 075422 (2017).

[17] G. Chen, L. Jiang, S. Wu, B. Lyu, H. Li, B. L. Chittari, K. Watanabe, T. Taniguchi, Z. Shi, J. Jung, Y. Zhang, and F. Wang, Evidence of a gate-tunable mott insulator in a trilayer graphene moiré superlattice, Nat. Phys. **15**, 237 (2019).

[18] Y. Lee, S. Che, J. Velasco Jr., D. Tran, J. Baima, F. Mauri, M. Calandra, M. Bockrath, and C. N. Lau, Gate tunable magnetism and giant magnetoresistance in abc-stacked few-layer graphene, arXiv:1911.04450.

[19] L.-J. Yin, L.-J. Shi, S.-Y. Li, Y. Zhang, Z.-H. Guo, and L. He, High-Magnetic-Field Tunneling Spectra of *abc*-Stacked Trilayer Graphene on Graphite, Phys. Rev. Lett. **122**, 146802 (2019).

[20] B. L. Chittari, G. Chen, Y. Zhang, F. Wang, and J. Jung, Gate-Tunable Topological Flat Bands in Trilayer Graphene Boron-Nitride Moiré Superlattices, Phys. Rev. Lett. **122**, 016401 (2019).

[21] G. Chen, A. L. Sharpe, P. Gallagher, I. T. Rosen, E. J. Fox, L. Jiang, B. Lyu, H. Li, K. Watanabe, T. Taniguchi, J. Jung, Z. Shi, D. Goldhaber-Gordon, Y. Zhang, and F. Wang, Signatures of tunable superconductivity in a trilayer graphene moiré superlattice, Nature (London) **572**, 215 (2019).

[22] G. Chen, A. L. Sharpe, E. J. Fox, Y.-H. Y. Zhang, S. Wang, L. Jiang, B. Lyu, H. Li, K. Watanabe, T. Taniguchi, Z. Shi, T. Senthil, D. Goldhaber-Gordon, Y.-H. Y. Zhang, and F. Wang, Tunable correlated chern insulator and ferromagnetism in trilayer graphene/boron nitride moiré superlattice, Nature (London) **579**, 56 (2020).

[23] Y. Shi, S. Xu, Y. Yang, S. Slizovskiy, S. V. Morozov, S.-K. Son, S. Ozdemir, C. Mullan, J. Barrier, J. Yin, A. I. Berdyugin, B. A. Piot, T. Taniguchi, K. Watanabe, V. I. Fal'ko, K. S. Novoselov, A. K. Geim, and A. Mishchenko, Electronic phase separation in multilayer rhombohedral graphite, Nature (London) **584**, 210 (2020).

[24] H. Zhou, T. Xie, A. Ghazaryan, T. Holder, J. R. Ehrets, E. M. Spanton, T. Taniguchi, K. Watanabe, E. Berg, M. Serbyn, and

A. F. Young, Half and quarter metals in rhombohedral trilayer graphene, Nature **598** (2021) 429-433.

[25] N. P. Armitage, E. J. Mele, and A. Vishwanath, Weyl and dirac semimetals in three-dimensional solids, Rev. Mod. Phys. **90**, 015001 (2018).

[26] Y. Cao, V. Fatemi, A. Demir, S. Fang, S. L. Tomarken, J. Y. Luo, J. D. Sanchez-Yamagishi, K. Watanabe, T. Taniguchi, E. Kaxiras, R. C. Ashoori, and P. Jarillo-Herrero, Correlated insulator behaviour at half-filling in magic-angle graphene superlattices, Nature (London) **556**, 80 (2018).

[27] Y. Cao, V. Fatemi, S. Fang, K. Watanabe, T. Taniguchi, E. Kaxiras, and P. Jarillo-Herrero, Unconventional superconductivity in magic-angle graphene superlattices, Nature (London) **556**, 43 (2018).

[28] W. Kohn and J. M. Luttinger, New Mechanism for Superconductivity, Phys. Rev. Lett. **15**, 524 (1965).

[29] T. Cea and F. Guinea, Coulomb interaction, phonons, and superconductivity in twisted bilayer graphene, Proc. Natl. Acad. Sci. USA **118**, e2107874118 (2021).

[30] V. Tien Phong, P. A. Pantaleón, T. Cea, and F. Guinea, Band structure and superconductivity in twisted trilayer graphene, Phys. Rev. B **104**, L121116 (2021).

[31] A. A. Zibrov, P. Rao, C. Kometter, E. M. Spanton, J. I. A. Li, C. R. Dean, T. Taniguchi, K. Watanabe, M. Serbyn, and A. F. Young, Emergent Dirac Gullies and Gully-Symmetry-Breaking Quantum Hall States in *aba* Trilayer Graphene, Phys. Rev. Lett. **121**, 167601 (2018).

[32] See Supplemental Material at http://link.aps.org/supplemental/10.1103/PhysRevB.105.075432 for the band structure of rhombohedral trilayer graphene and a comparison of tight-binding and continuum models.

[33] T. O. Wehling, E. Şaşıoğlu, C. Friedrich, A. I. Lichtenstein, M. I. Katsnelson, and S. Blügel, Strength of Effective Coulomb Interactions in Graphene and Graphite, Phys. Rev. Lett. **106**, 236805 (2011).

[34] Note that we consider solely the Coulomb interaction associated with the fluctuations of the total charge density. The inclusion of a spin-dependent, intervalley Hund coupling can allow for the existence of singlet solutions [5,6].